Analysis of Nuclear Quantum Effects on Hydrogen Bonding

Chet Swalina, Qian Wang, Arindam Chakraborty, and Sharon Hammes-Schiffer*

Department of Chemistry, 104 Chemistry Building, Pennsylvania State University, University Park, Pennsylvania 16802

Received: December 1, 2006; In Final Form: January 11, 2007

The impact of nuclear quantum effects on hydrogen bonding is investigated for a series of hydrogen fluoride $(HF)_n$ clusters and a partially solvated fluoride anion, $F^-(H_2O)$. The nuclear quantum effects are included using the path integral formalism in conjunction with the Car−Parrinello molecular dynamics (PICPMD) method and using the second-order vibrational perturbation theory (VPT2) approach. For the HF clusters, a directional change in the impact of nuclear quantum effects on the hydrogen-bonding strength is observed as the clusters evolve toward the condensed phase. Specifically, the inclusion of nuclear quantum effects increases the F−F distances for the $(HF)_{n=2-4}$ clusters and decreases the F−F distances for the $(HF)_{n>4}$ clusters. This directional change occurs because the enhanced electrostatic interactions between the HF monomers become more dominant than the zero point energy effects of librational modes as the size of the HF clusters increases. For the $F^-(H_2O)$ system, the inclusion of nuclear quantum effects decreases the F−O distance and strengthens the hydrogen bonding interaction between the fluoride anion and the water molecule because of enhanced electrostatic interactions. The vibrationally averaged ^{19}F shielding constant for $F^-(H_2O)$ is significantly lower than the value for the equilibrium geometry, indicating that the electronic density on the fluorine decreases as a result of the quantum delocalization of the shared hydrogen. Deuteration of this system leads to an increase in the vibrationally averaged F−O distance and nuclear magnetic shielding constant because of the smaller degree of quantum delocalization for deuterium.

I. Introduction

Hydrogen bonding plays a vital role throughout chemistry and biology. Nuclear quantum effects such as zero-point energy and tunneling have been shown to influence the structural and dynamical properties of hydrogen bonds. A wide range of computational methods have been developed to include nuclear quantum effects in calculations of hydrogen-bonded systems in both the gas phase and condensed phases. Applications of computational methods to model systems such as hydrogen fluoride (HF) and water have provided insights into the quantum mechanical nature of hydrogen bonds.[1−14]

The impact of nuclear quantum effects on the structure of hydrogen-bonded liquids has been studied with the density functional theory-based Car−Parrinello molecular dynamics (CPMD) method in conjunction with the Feynman path integral (PI) treatment of the nuclei. For both liquid HF and water, inclusion of nuclear quantum effects with the PICPMD method resulted in shorter hydrogen bond donor−acceptor distances compared to the corresponding classical CPMD simulations.[6,7] The shorter donor−acceptor distances in the PICPMD simulations reflect strengthened hydrogen bonds arising from enhanced electrostatic interactions between individual monomers. The anharmonicity of the potential and the corresponding delocalization of the hydrogen nuclei increase the dipole moments in the individual monomers, resulting in enhanced electrostatic interactions.

The impact of nuclear quantum effects on the structures of gas-phase hydrogen-bonded clusters has been investigated with a variety of methods. Nuclear quantum effects on water clusters have been studied with the quantum diffusion Monte Carlo approach.[8,9] In contrast to the results obtained with the PICPMD method for liquid water, the inclusion of nuclear quantum effects in gas-phase water clusters produced increased O−O distances for clusters containing up to six water molecules. Nuclear quantum effects were also found to increase the O−O distance in the water dimer using a different method for including the intermolecular part of the zero point vibrational energy.[10] Furthermore, the inclusion of nuclear quantum effects in the HF dimer with the second-order vibrational perturbation theory (VPT2) method resulted in an increased F−F distance that is consistent with experiment.[11,15] This increase in the F−F distance of the HF dimer is due to the librational, or bending-type, modes. As the separation between the two HF monomers is decreased slightly from equilibrium, the bending motion becomes more confined, increasing the zero point energy of this mode. In contrast, the stretching potential of the shared hydrogen becomes flatter, reducing the zero point energy of this mode. The vibrationally averaged F−F distance is determined by a balance between the opposing effects of the bending and stretching modes, as well as the electrostatic effects. The same combination of effects also leads to increased O−O distances in the water dimer.[10]

In this paper, we investigate the impact of nuclear quantum effects on hydrogen bonding in a series of HF clusters and the $F^-(H_2O)$ system. The HF clusters represent relatively weakly bound systems, and $F^-(H_2O)$ represents a relatively tightly bound system. Specifically, the dissociation energy D_0 for $F^-(H_2O)$ is 26.2 ± 0.8 kcal/mol,[16] and the dissociation energy D_0 for $(HF)_2$ is 4.6 kcal/mol.[17] Our study of the HF clusters

* Corresponding author. E-mail: shs@chem.psu.edu.

10.1021/jp0682661 CCC: $37.00
Published on Web 02/24/2007

was motivated by the previous observations that nuclear quantum effects decrease the hydrogen bond strength (i.e., increase the donor−acceptor distances) for small gas-phase clusters and enhance the hydrogen bond strength (i.e., decrease the donor−acceptor distances) for liquid HF and water. Our objective was to determine if the impact of nuclear quantum effects on the donor−acceptor distances changes directionality as the cluster size increases and to analyze the balance of effects leading to this type of crossover behavior. The partially solvated fluoride anion, $F^-(H_2O)$, is more strongly bound than the HF clusters, and the hydrogen bond is dominated by electrostatic interactions. As a result, a more detailed analysis of the nuclear quantum effects can be performed for $F^-(H_2O)$. In particular, the vibrationally averaged nuclear magnetic shielding constants can be calculated for this system to elucidate the impact of nuclear quantum effects on the electronic structure. The combined study of these two types of systems presented in this paper provides insight into the fundamental quantum mechanical nature of hydrogen bonds.

II. Methods

We utilized two different approaches to study the impact of nuclear quantum effects on the structural properties of HF clusters. The first approach is the density functional theory-based Car−Parrinello molecular dynamics (CPMD) method,[18] in which the nuclei move on a potential energy surface generated "on the fly." To study the impact of nuclear quantum effects, we performed the CPMD simulations with both a classical treatment of the nuclei and a Feynman path integral (PI) quantum treatment of the nuclei.[19,20] In the discrete path integral formalism, each quantum nucleus is represented by a ring of p quasiparticles, where each quasiparticle interacts with its two neighbors via a harmonic potential and experiences $1/p$ of the actual potential energy. Equilibrium quantum mechanical average quantities are obtained through molecular dynamics simulation of the system of quasiparticles. The second approach is the second-order vibrational perturbation theory (VPT2) method,[21,22] in which zero-order vibrational wave functions are generated from the harmonic approximation, and second-order perturbation theory corrections are calculated from the cubic and semidiagonal quartic force constants. The VPT2 method enables the calculation of vibrationally averaged molecular properties that include anharmonic effects for comparison to the corresponding properties of the equilibrium structures. We chose the PICPMD and VPT2 methods because they are based on well-defined approximations and are computationally practical for these systems.

The PICPMD and CPMD simulations were performed with the PINY_MD[23,24] simulation package at 290 K with a 0.1 fs time step. The temperature of 290 K, which is slightly below the HF liquid boiling point of 292.7 K at 1 atm,[25] was chosen to be consistent with the HF liquid PICPMD simulations of Raugei and Klein.[6] The BLYP exchange-correlation functional was utilized for these simulations. Troullier−Martins type pseudopotentials were used for the hydrogen atoms and the atomic core of the fluorine atoms.[26] The valence wavefunctions were expanded in a plane wave basis set with an energy cutoff of 80 Ry. To test the effect of the cutoff, the calculations were also performed for the HF dimer and trimer with an energy cutoff of 90 Ry. The overall trends were found to be the same for the two values of the energy cutoff. For the PICPMD simulations, each quantum nucleus was represented by a ring of $p = 16$ quasiparticles. Qualitatively similar results were obtained using $p = 8$ quasiparticles. The CPMD data for the classical nuclei were obtained by averaging the distances over 20 ps after an equilibration of 3 ps for the dimer and trimer and by averaging the distances over 9 ps after an equilibration of 3 ps for the larger clusters. The PICPMD data with $p = 16$ were obtained by averaging the distances over 1 ps (i.e., 10 000 time steps) following 1 ps of equilibration for each HF cluster. To test the convergence, the PICPMD simulations were also performed with $p = 8$ quasiparticles, averaging the distances over 5 ps following 3 ps of equilibration for $(HF)_2$ and $(HF)_3$, averaging the distances over 1.5 ps following 1 ps of equilibration for $(HF)_4$ and $(HF)_5$, and averaging the distances over 1 ps following 1 ps of equilibration for $(HF)_6$. Similar results were obtained from these additional simulations.

The VPT2 calculations for the HF clusters were performed using the implementation[21,22] in Gaussian03[27] with density functional theory in conjunction with both the BLYP[28,29] and B3LYP[30,31] exchange-correlation functionals. The aug-cc-pVDZ[32] basis set was used for all of these calculations. We verified that this electronic basis set is sufficient by calculating the difference between vibrationally averaged and equilibrium F−F and F−H distances for the HF trimer at the BLYP level using a series of basis sets, aug-cc-pVnZ for $n = 2-4$. The differences in these distances for this series of basis sets were less than 0.003 Å. An ultrafine grid was used for the numerical quadrature in the Kohn−Sham procedure, and the geometries were optimized using a tolerance of 10^{-6} Hartree/Bohr. The displacement size used for the numerical differentiation of analytical second derivatives in the VPT2 procedure was 0.01 Å.

We used two different implementations of the VPT2 approach to study the nuclear quantum effects in $F^-(H_2O)$. The VPT2 method as implemented by Barone[21,22] in Gaussian03[27] was used to calculate anharmonic vibrational frequencies. In addition, the vibrationally averaged molecular structures and isotropic nuclear magnetic shielding constants were calculated using the VPT2 approach as implemented[33−35] in the DALTON[36] electronic structure program. Note that the Hessian eigenvalue threshholds used to distinguish vibrations from rotations and translations needed to be increased slightly at the DFT level in order to perform the VPT2 calculations in DALTON. For this system, all calculations were performed with density functional theory at the B3LYP/aug-cc-pVTZ level of theory.

III. Results

A. Hydrogen Fluoride Clusters. The structures for the series of HF clusters were calculated at the B3LYP/aug-cc-pVDZ level and are depicted in Figure 1. These structures are cyclic,[37,38] whereas the liquid form of HF consists of zigzag hydrogen-bonded chains.[6] As the HF clusters increase in size, however, they can acquire characteristics present in the liquid because the larger rings are approximately zigzag hydrogen-bonded chains that are connected at both ends. Thus, the investigation of this series of HF clusters can provide insight into the qualitatively different behavior of small gas-phase HF clusters and liquid HF. As discussed above, the inclusion of nuclear quantum effects was previously found to increase the F−F distance for the HF dimer and decrease the F−F distances for liquid HF.

The impact of nuclear quantum effects on the donor−acceptor F−F distances in the $(HF)_n$ clusters is calculated as

$$\Delta R_{FF}(n) = R^Q_{FF}(n) - R^C_{FF}(n) \quad (1)$$

The superscript Q indicates that the F−F distance was calculated with the PICPMD or VPT2 method, whereas the superscript C

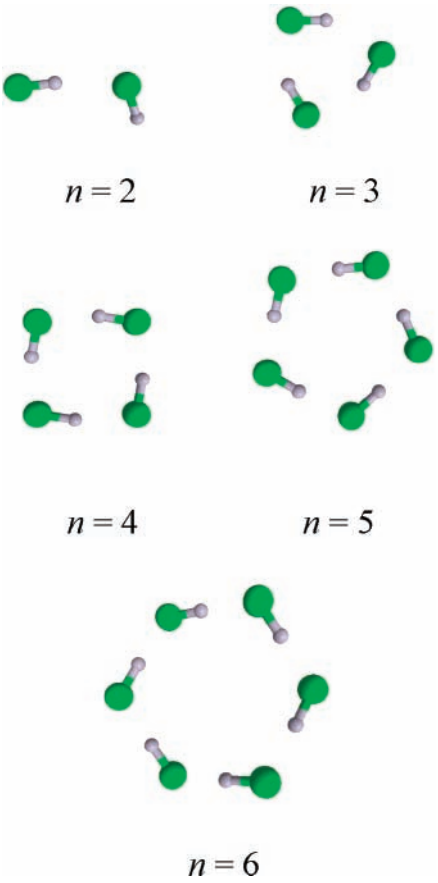

Figure 1. Structures of hydrogen fluoride clusters, $(HF)_{n=2-6}$, calculated at the B3LYP/aug-cc-pVDZ level.

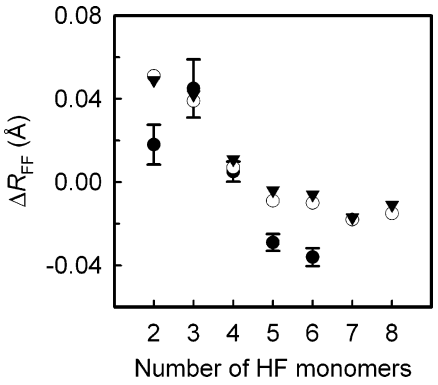

Figure 2. Difference between quantum and classical F−F distances for a series of hydrogen fluoride clusters. ΔR_{FF} is defined in eq 1. The filled circles correspond to CPMD calculations, the open circles correspond to VPT2/BLYP calculations, and the filled triangles correspond to VPT2/B3LYP calculations. The error bars correspond to the standard error of the mean with correlation corrections[48,49] computed for the PICPMD and CPMD simulations. The error is reduced for the larger HF clusters since they are more strongly bound.

indicates that the F−F distance was calculated using the classical CPMD method or the equilibrium value from a conventional electronic structure optimization. An analogous expression is used for the covalent F−H distances in these clusters.

The impact of nuclear quantum effects on the F−F distances for the clusters $(HF)_{n=2-6}$ is depicted in Figure 2. The inclusion of nuclear quantum effects increases the F−F distances for the $(HF)_{n=2-4}$ clusters and decreases the F−F distances for the $(HF)_{n>4}$ clusters. Thus, as the HF clusters evolve toward the condensed phase, a directional change in the impact of the nuclear quantum effects on the hydrogen-bonding strength

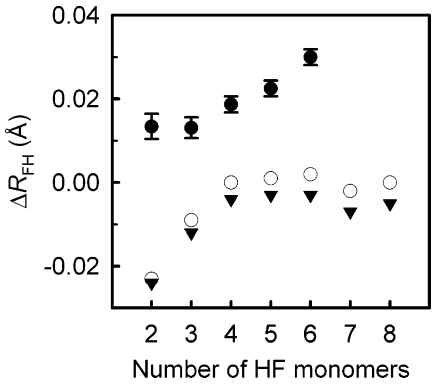

Figure 3. Difference between quantum and classical covalent F−H distances for a series of hydrogen fluoride clusters. ΔR_{FH} is defined analogously to ΔR_{FF} in eq 1. The filled circles correspond to CPMD calculations, the open circles correspond to VPT2/BLYP calculations, and the filled triangles correspond to VPT2/B3LYP calculations. The error bars correspond to the standard error of the mean with correlation corrections[48,49] computed for the PICPMD and CPMD simulations.

occurs between $(HF)_4$ and $(HF)_5$. The ΔR_{FF} values obtained with the VPT2 method agree well with the values obtained using the PICPMD method for the $(HF)_{n=3,4}$ clusters. The change in the sign of ΔR_{FF} between $(HF)_4$ and $(HF)_5$ is observed with both the VPT2 and PICPMD methods, but the quantitative ΔR_{FF} values differ for the dimer and the $(HF)_{n=5,6}$ clusters.

For the HF dimer, ΔR_{FF} is ~0.04 Å smaller for the PICPMD calculations than for the VPT2 calculations. This difference arises because the PICPMD simulations sample the two equivalent hydrogen-bonded conformers, whereas the VPT2 calculations are based on an expansion about a single equilibrium conformation. The VPT2 and PICPMD results for the HF dimer are qualitatively similar in that they both result in positive ΔR_{FF} values, indicating that the inclusion of nuclear quantum effects increases the F−F distance for the HF dimer. This observation is consistent with previous calculations illustrating that the inclusion of nuclear quantum effects increases the O−O distance for the water dimer.[10]

The quantitative differences between the VPT2 and PICPMD results for the ΔR_{FF} values in the $(HF)_{n=5,6}$ clusters can be understood by analyzing the ΔR_{FH} values depicted in Figure 3. At the PICPMD level, the ΔR_{FH} values are positive and increase with the size of the HF cluster for $n = 3 - 6$. In contrast, at the VPT2 level, the ΔR_{FH} values are negative and do not display a clear trend with cluster size. In general, the F−H distances are expected to increase upon inclusion of nuclear quantum effects due to the anharmonicities of the F−H stretching modes. The PICPMD results follow this expected trend. The non-physical contraction of the F−H distances obtained with the VPT2 method is largely responsible for the quantitative differences in the ΔR_{FF} values for the larger clusters. The Appendix presents an analysis that addresses this contraction of the F−H distances at the VPT2 level. This analysis indicates that the nonphysical contraction of the vibrationally averaged F−H distances arises from the truncation of the poorly converging many-mode potential. This issue casts doubt on the quantitative reliability of the VPT2 results for these types of systems. Finite temperature effects may also lead to differences between the VPT2 and PICPMD methods.

The directional change in the impact of nuclear quantum effects on the hydrogen bonding in the HF clusters is due to a competition between two effects. In the smaller clusters, zero point energy contributions stemming from vibrational modes are the dominant factor, leading to an increase in the distances

Figure 4. Structure of the $F^-(H_2O)$ system calculated at the B3LYP/aug-cc-pVTZ level.

TABLE 1: Calculated and Experimental Vibrational Frequencies in cm^{-1} for $F^-(H_2O)$ and $F^-(D_2O)$[a]

mode[b]	$F^-(H_2O)$ harmonic	$F^-(H_2O)$ VPT2	$F^-(D_2O)$ harmonic	$F^-(D_2O)$ VPT2	experiment[c]
ν_{iw}	390	408	375	384	–
ν_{ip}	574	568	416	411	–
ν_{oop}	1146	1010	823	713	1083-1250
ν_b	1689	1607	1228	1188	1650
ν_{IHB}	2138	1088	1569	982	1523
ν_f	3849	3664	2800	2701	3687

[a] Calculated values obtained at the B3LYP/aug-cc-pVTZ level. [b] Modes have been assigned according to ref 47: ν_{iw}, ion-water stretch; ν_{ip}, in-plane wag; ν_{oop}, out-of-plane wag; ν_b, HOH bend; ν_{IHB}, ionic hydrogen bond; ν_f, free OH stretch. [c] Ref 47 for $F^-(H_2O)$.

between HF monomers. For the larger HF clusters, enhanced electrostatic interactions between the HF monomers become the dominant factor, leading to a decrease in the distances between HF monomers. As shown from previous conventional electronic structure calculations[12] and CPMD calculations,[6] the electrostatic interactions between the HF monomers become more dominant in the larger HF clusters because of an increase in the net molecular dipole moment. In particular, electronic density shifts from the hydrogen atoms to the fluorine atoms and the F−H bond length increases as the HF clusters increase in size from $n = 2$ to $n = 6$. Similarly, the increase of the PICPMD ΔR_{FH} values with cluster size indicates that the anharmonicities of the F−H stretching modes increase with cluster size in this regime. When the electrostatic interactions dominate, the enhanced electrostatic interactions between the HF monomers arising from the anharmonicities of the F−H modes and the corresponding quantum delocalization of the hydrogen nuclei lead to a decrease in the F−F distance.

B. Partially Solvated Fluoride Anion, $F^-(H_2O)$. In this section we present an analysis of the impact of nuclear quantum effects on hydrogen bonding for the $F^-(H_2O)$ system depicted in Figure 4. In contrast to the HF clusters, the vibrationally averaged covalent O−H distances calculated with the VPT2 method for $F^-(H_2O)$ are not contracted relative to the equilibrium values. Thus, the VPT2 method can be used to examine the impact of nuclear quantum effects for this system. In addition, a more detailed analysis can be performed for this system by calculating vibrationally averaged isotropic nuclear magnetic shielding constants with the VPT2 approach.

The harmonic and anharmonic vibrational frequencies for the $F^-(H_2O)$ system and its deuterated analog, $F^-(D_2O)$, are given in Table 1. For the $F^-(H_2O)$ system, the anharmonic correction is greater than 1000 cm^{-1} for the hydrogen stretching mode involving the ionic hydrogen bond. The anharmonic correction for the corresponding mode in the $F^-(D_2O)$ system is also substantial. For both systems, this correction is significantly greater than the anharmonic corrections for the other vibrational frequencies. The large anharmonic correction indicates that the shared hydrogen (or deuterium) is significantly delocalized between the oxygen and the fluorine atoms due to the anharmonicity in the potential for this mode.

TABLE 2: Equilibrium and Vibrationally Averaged Structural Parameters for $F^-(H_2O)$ and $F^-(D_2O)$[a]

	R_{FO}	R_{FH_b}	R_{OH_b}	R_{OH_f}
equilibrium[b]	2.4496	1.3874	1.0629	0.9600
vib. av. $F^-(H_2O)$[c]	2.4320	1.3300	1.1024	0.9646
vib. av. $F^-(D_2O)$[c]	2.4422	1.3523	1.0904	0.9636

[a] H_b denotes the shared hydrogen, and H_f denotes the free hydrogen. All values are in Å. [b] Structural parameters for the equilibrium geometry optimized at the B3LYP/aug-cc-pVTZ level. [c] Vibrationally averaged structural parameters calculated with the VPT2 method at the B3LYP/aug-cc-pVTZ level.

TABLE 3: Equilibrium and Vibrationally Averaged Isotropic Nuclear Magnetic Shielding Constants for $F^-(H_2O)$ and $F^-(D_2O)$[a]

	^{19}F	^{17}O	H_b	H_f
equilibrium[b]	396.20	307.37	17.15	33.73
vib. av. $F^-(H2O)$[c]	387.43	299.15	16.52	33.71
vib. av. $F^-(D2O)$[c]	389.62	299.38	16.85	33.65

[a] H_b denotes the shared hydrogen, and H_f denotes the free hydrogen. All values are in ppm. [b] Shielding constants for the equilibrium geometry optimized at the B3LYP/aug-cc-pVTZ level. [c] Vibrationally averaged shielding constants calculated with the VPT2 method at the B3LYP/aug-cc-pVTZ level.

The equilibrium and vibrationally averaged structural parameters for the $F^-(H_2O)$ and $F^-(D_2O)$ systems are given in Table 2. The O−H_b distance, where H_b denotes the shared hydrogen, increases by ∼0.04 Å upon inclusion of the nuclear quantum effects. The corresponding O−D_b distance increases by ∼0.03 Å. These trends are qualitatively consistent with the anharmonic corrections to the vibrational frequencies given in Table 1. The F−H_b hydrogen bond distances decrease by 0.057 and 0.035 Å, respectively, for the $F^-(H_2O)$ and $F^-(D_2O)$ systems. The F−O distances exhibit similar trends.

These trends in the frequencies and structures indicate that the nuclear quantum effects enhance the interaction between the fluoride anion and the water molecule. For these systems, the electrostatic interactions are the dominant factor in determining the impact of the nuclear quantum effects. Specifically, inclusion of the nuclear quantum effects of the shared hydrogen increases the vibrationally averaged O−H_b bond length relative to its equilibrium value and leads to greater charge separation in this bond, thereby increasing the electrostatic interaction between the fluoride anion and the water molecule. This enhanced electrostatic interaction decreases the F−O and F−H_b distances in the hydrogen bond. These effects are greater for hydrogen than for deuterium due to the smaller mass and correspondingly greater delocalization of hydrogen.

These physical phenomena can be further analyzed by calculating the vibrationally averaged isotropic nuclear magnetic shielding constants, which are sensitive to the electronic environments around the nuclei. In general, the nuclear magnetic shielding constant is greater for higher electronic density about the nucleus. The equilibrium and vibrationally averaged isotropic nuclear magnetic shielding constants for $F^-(H_2O)$ and $F^-(D_2O)$ are given in Table 3. The difference between the ^{19}F shielding constants for $F^-(H_2O)$ and $F^-(D_2O)$ is 2.2 ppm. This value differs by less than 1 ppm from the experimentally measured H/D isotope effect of 3.0 ± 0.1 ppm on the ^{19}F shielding constant for the fluoride anion in solution.[39] In order to explore the effect of solvation for the H/D isotope effect on the ^{19}F shielding constant, we performed a VPT2 analysis on $F^-(H_2O)_2$. Unfortunately, the VPT2 method leads to nonphysical contractions of the O−H distances in the $F^-(H_2O)_2$ system for reasons discussed in the Appendix. Thus, the VPT2 method is not

reliable for the analysis of the vibrationally averaged magnetic properties of the $F^-(H_2O)_2$ system. Nevertheless, the agreement between the experimental isotope effect and the calculated value for the system in which the fluoride anion is solvated by only a single water molecule indicates that the VPT2 analysis is physically reasonable for this system.

The trends in the calculated isotropic nuclear magnetic shielding constants provide additional insight into the impact of the nuclear quantum effects on the $F^-(H_2O)$ system. The vibrationally averaged ^{19}F shielding constant is ~9 ppm lower than the ^{19}F shielding constant evaluated for the equilibrium geometry. This decrease in the shielding constant indicates a decrease in the electronic density on the fluorine upon inclusion of nuclear quantum effects. This lower electronic density on the fluorine is consistent with the structural analysis above. In particular, the enhanced electrostatic interaction between the fluoride anion and the water molecule upon inclusion of nuclear quantum effects leads to a decrease in the electronic density on the fluorine. The ^{19}F shielding constant is lower for H_2O than for D_2O because the proton is more delocalized than the deuteron in the hydrogen bond, resulting in greater electrostatic interactions in the $F^-(H_2O)$ system. All of these analyses indicate that including the nuclear quantum effects enhances the hydrogen bonding interaction between the fluoride anion and the water molecule.

IV. Conclusions

In this paper, the impact of nuclear quantum effects on hydrogen bonding was investigated for two types of hydrogen-bonded systems, $(HF)_{n=2-6}$ and $F^-(H_2O)$. The PICPMD and VPT2 methods were used to study the HF clusters, and the VPT2 method was used to study $F^-(H_2O)$. Both methods provided qualitatively similar results for the changes in hydrogen-bonding strength with HF cluster size. The VPT2 method, however, resulted in a nonphysical contraction of the vibrationally averaged F−H distances relative to the equilibrium values in the HF clusters. An analysis of the HF dimer with the VSCF method indicated that the practical application of the VSCF and VPT2 methods to HF clusters is problematic because of the truncation of a poorly converging expansion series. In contrast, the VPT2 method was found to be physically reasonable for the $F^-(H_2O)$ system, which is more tightly bound than the HF clusters. Additional insights into the $F^-(H_2O)$ system were provided by a VPT2 analysis of the vibrationally averaged isotropic nuclear magnetic shielding constants.

For the HF clusters, the calculations identified a directional change in the impact of nuclear quantum effects on the hydrogen-bonding strength as the HF clusters evolved toward the condensed phase. In particular, the inclusion of nuclear quantum effects increases the F−F distances for the $(HF)_{n=2-4}$ clusters and decreases the F−F distances for the $(HF)_{n>4}$ clusters. The largest distance change observed for these clusters is ~0.04 Å. The directional change that occurs between $(HF)_4$ and $(HF)_5$ arises from a competition between zero point energy effects of librational modes and enhanced electrostatic interactions between the HF monomers arising from delocalization of the quantum protons. The zero point energy effects of librational modes tend to increase the F−F distances because the zero point energy of this mode decreases as the separation between the two HF monomers is increased slightly from equilibrium. In contrast, the enhancement of the electrostatic interactions between the HF monomers due to nuclear quantum effects tends to decrease the F−F distances. The physical basis for this enhancement is that the nuclear quantum effects lead to an increase in the vibrationally averaged F−H bond length relative to the equilibrium bond length and a greater charge separation within the HF monomers, thereby enhancing the electrostatic interactions between the HF monomers. The electrostatic effects become more dominant as the size of the HF clusters increases because of the shift in electronic density from the hydrogen atoms to the fluorine atoms and the increase in F−H bond length with cluster size. These calculations provide a physical explanation for the previous observations that nuclear quantum effects weaken the hydrogen bonding interactions in small gas-phase clusters but strengthen the hydrogen bonding interactions in hydrogen-bonded liquids.

For the $F^-(H_2O)$ system, the inclusion of nuclear quantum effects strengthen the hydrogen bonding interaction between the fluoride anion and the water molecule because of enhanced electrostatic interactions. A large anharmonic red shift of ~1000 cm^{-1} was calculated for the vibrational stretching frequency corresponding to the shared hydrogen. In addition, the donor−acceptor F−O distance decreased by ~0.02 Å and the covalent O−H distance for the shared hydrogen increased by ~0.04 Å upon inclusion of nuclear quantum effects. These effects were also observed for the $F^-(D_2O)$ system, but the degree of electrostatic enhancement and corresponding strengthening of the hydrogen bond was less pronounced. The resulting H/D isotope effect for the structural and vibrational properties is consistent with the Ubbelohde effect[40] observed for crystals. An analysis of the vibrationally averaged isotropic nuclear magnetic shielding constants provided insight into the impact of nuclear quantum effects on the electronic structure of this system. The vibrationally averaged ^{19}F shielding constant for $F^-(H_2O)$ was significantly lower than the value for the equilibrium geometry, indicating that the electronic density on the fluorine decreases as a result of the quantum delocalization of the shared hydrogen. This effect was observed for the $F^-(D_2O)$ system to a lesser extent. The H/D isotope effect on the ^{19}F shielding constant was within 1 ppm of the experimental[39] value of 3.0 ppm for the fluoride anion in solution. These trends for the vibrationally averaged ^{19}F shielding constants confirm that the inclusion of nuclear quantum effects enhances the electrostatic interactions between the fluoride anion and the water molecule.

This analysis of nuclear quantum effects in hydrogen-bonded systems provides insight into the fundamental physical principles dictating the quantum mechanical behavior of hydrogen bonds. The qualitative impact of nuclear quantum effects on hydrogen bonding depends on the underlying electronic structure of the system. The quantum delocalization of the protons tends to strengthen the hydrogen bonds for relatively strongly bound systems with polarizable hydrogen bond acceptors and to weaken the hydrogen bonds for relatively weakly bound systems with less polarizable hydrogen bond acceptors. These effects could be significant for simulations of hydrogen-bonded systems in both the gas phase and condensed phases.

Appendix

This appendix presents an analysis of the cause of the nonphysical contraction of the VPT2 vibrationally averaged F−H distances in the HF clusters. We used the related vibrational self-consistent field (VSCF) approach[41−44] to examine this issue. In the VSCF approach, the *N*-dimensional vibrational wavefunction for an *N*-mode system is represented as a product of *N* single-mode vibrational wavefunctions, and the *N*-dimensional vibrational Schrödinger equation reduces to the self-consistent solution of *N* single-mode vibrational equa-

TABLE A1: Calculated Vibrational Frequencies in cm^{-1} for the HF Dimer[a]

mode	VSCF(1)	VSCF(2)	VSCF(3)	harmonic
stretch	3847	3790	3777	4016
stretch	3683	3627	3607	3882
bend	782	745	715	578
o/p bend	789	686	567	465
bend	584	547	500	233
F−F stretch	220	246	257	167

[a] The calculations were performed at the B3LYP/aug-cc-pVDZ level. The VSCF(*n*) method includes up to *n*-order terms in the many-mode expansion of the VSCF potential.

TABLE A2: Calculated Structural Parameters for the HF Dimer[a]

method	R_{FF}	R_{FH_b}[b]	R_{FH_f}[b]
equilibrium	2.7320	0.9337	0.9289
VSCF(1)	2.7397	0.9492	0.9469
VSCF(2)	2.7532	0.9324	0.9322
VSCF(3)	2.7506	0.9304	0.9263

[a] The calculations were performed at the B3LYP/aug-cc-pVDZ level. The VSCF(*n*) method includes up to *n*-order terms in the many-mode expansion of the VSCF potential. All values are in Å. [b] H_b denotes the shared hydrogen, and H_f denotes the free hydrogen.

tions. For six-mode systems such as $(HF)_2$ and $F^-(H_2O)$, the full many-mode potential is

$$V(Q_1,Q_2,...,Q_6) = \sum_i V_i^{(1)}(Q_i) + \sum_{i<j} V_{ij}^{(2)}(Q_i,Q_j) + \sum_{i<j<k} V_{ijk}^{(3)}(Q_i,Q_j,Q_k) + \sum_{i<j<k<l} V_{ijkl}^{(4)}(Q_i,Q_j,Q_k,Q_l) + \sum_{i<j<k<l<m} V_{ijklm}^{(5)}(Q_i,Q_j,Q_k,Q_l,Q_m) + \sum_{i<j<k<l<m<n} V_{ijklmn}^{(6)}(Q_i,Q_j,Q_k,Q_l,Q_m,Q_n) = U^{(1)} + U^{(2)} + U^{(3)} + U^{(4)} + U^{(5)} + U^{(6)} \quad \text{(A.1)}$$

where $U^{(n)}$ corresponds to the sum over all *n*-order terms. In practical implementations based on direct computation of the VSCF quadrature points with electronic structure theory methods,[43,45] the VSCF many-mode potential in eq A.1 is typically truncated to include up to the first three terms (i.e., up to third-order terms). An analogous truncation occurs in the VPT2 method.

We performed a series of VSCF calculations including one-, two-, and three-order terms in the many-mode potential in eq A.1 for the HF dimer and the partially solvated fluoride anion, $F^-(H_2O)$. These calculations were performed using the VSCF method[43,45] implemented in the GAMESS[46] electronic structure program. For all calculations, 16 directly computed quadrature points along each mode were used to construct the $VSCF(n)_{n=1-3}$ many-mode potentials at the B3LYP/aug-cc-pVDZ level.

The frequencies and vibrationally averaged structural parameters for the HF dimer are given in Tables A1 and A2, respectively. In this weakly bound system, four of the six modes have frequencies that are less than 1000 cm^{-1}. For these four low-frequency modes, all of the VSCF calculations produce frequencies that are significantly greater than the corresponding harmonic values. This trend indicates that the truncated VSCF potentials used in these calculations contain attractive contributions involving the low-frequency modes. The vibrationally averaged covalent F−H distances computed at the VSCF(2) and VSCF(3) levels are contracted relative to the corresponding equilibrium (i.e., harmonic) values. Thus, the VSCF approach exhibits the same non-physical behavior as the VPT2 approach for the HF dimer.

TABLE A3: Calculated Vibrational Frequencies in cm^{-1} for the $F^-(H_2O)$ System[a]

mode	VSCF(1)	VSCF(2)	VSCF(3)	harmonic
1	3680	3620	3625	3845
2	1649	1618	1629	2216
3	1657	1617	1619	1676
4	1166	1126	1130	1122
5	729	612	624	461
6	376	421	420	387

[a] The calculations were performed at the B3LYP/aug-cc-pVDZ level. The VSCF(*n*) method includes up to *n*-order terms in the many-mode expansion of the VSCF potential.

TABLE A4: Calculated Structural Parameters for the $F^-(H_2O)$ System[a]

method	R_{FO}	R_{FH_b}[b]	R_{OH_b}[b]	R_{OH_f}[b]
equilibrium	2.4645	1.4059	1.0600	0.9632
VSCF(1)	2.4818	1.3760	1.1080	0.98
VSCF(2)	2.4576	1.3569	1.1012	0.9707
VSCF(3)	2.4563	1.3545	1.1025	0.9710

[a] The calculations were performed at the B3LYP/aug-cc-pVDZ level. The VSCF(*n*) method includes up to *n*-order terms in the many-mode expansion of the VSCF potential. All values are in Å. [b] H_b denotes the shared hydrogen, and H_f denotes the free hydrogen.

The frequencies and vibrationally averaged structural parameters for the $F^-(H_2O)$ system are given in Tables A3 and A4, respectively. Since this system is more tightly bound than the HF dimer, only two of the six modes have frequencies that are less than 1000 cm^{-1}. As observed for the HF dimer, the VSCF calculations produce frequencies that are higher than the corresponding harmonic values for these two low-frequency modes. The vibrationally averaged covalent O−H distances computed at the $VSCF(n)_{n=1,2,3}$ levels are greater than the corresponding equilibrium (i.e., harmonic) values. Thus, the VSCF and VPT2 approaches do not exhibit the non-physical contraction of the O−H distances for this system.

To obtain further insight into the behavior of the higher-order terms in the VSCF many-mode potentials for the $(HF)_2$ and $F^-(H_2O)$ systems, we evaluated the $VSCF(n)_{n=1-6}$ potential for a single point in displaced normal mode coordinates for both systems. For convenience, we used the vibrationally averaged geometry calculated at the VSCF(2)/B3LYP/aug-cc-pVDZ level for each system. The values of each of the six terms comprising the full many-mode potential in Equation A.1 evaluated at this single point are depicted in Figure A1. The higher-order terms in the many-mode expansion are up to 3 orders of magnitude larger for the HF dimer than for the $F^-(H_2O)$ system. Moreover, the second and fourth terms in the many-mode potential for the HF dimer are negative, indicating an attractive contribution to the overall potential. The oscillatory behavior of the terms in the many-mode potential, as well as the larger magnitudes of the higher-order terms ($n = 2-4$) than the first-order term, were also observed at the MP2/aug-cc-pVTZ level of theory. These MP2 data are provided in Supporting Information. Thus, the many-mode potential converges non-monotonically for the HF dimer at both the DFT and MP2 levels of electronic structure theory.

This analysis indicates that the non-physical contraction of the vibrationally averaged F−H distances in the HF clusters arises from the truncation of the full many-mode potential in the VSCF approach. The analogous truncation in the VPT2

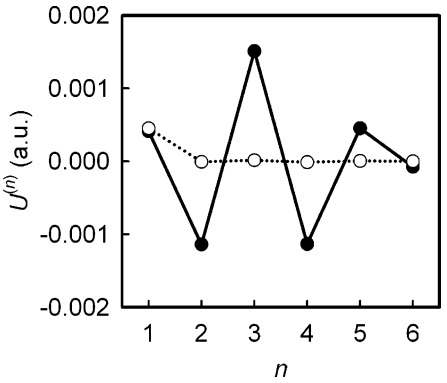

Figure A1. Individual *n*-order terms comprising the full many-mode potential at a single point in displaced normal mode coordinates for $(HF)_2$ (closed circles) and $F^-(H_2O)$ (open circles) at the B3LYP/aug-cc-pVDZ level. For each system, the single point was chosen to be the vibrationally averaged geometry calculated at the VSCF(2)-B3LYP/aug-cc-pVDZ level.

approach also leads to these non-physical contractions. The convergence problems are expected to be more significant for weakly bound systems with low-frequency modes. Since the $F^-(H_2O)$ system is more tightly bound and contains fewer low-frequency modes than the HF dimer, the many-mode potential converges better, and the truncation of the potential is a reasonable approximation for this system. Vibrationally averaged structural effects such as the contraction of F−H distances can be used as a diagnostic for identifying non-convergent behavior of the VSCF and VPT2 methods for hydrogen-bonded systems.

Acknowledgment. We gratefully acknowledge the support of AFOSR grant FA9550-04-1-0062 and NSF grant CHE-05-01260. C. S. acknowledges support from a Lubrizol Fellowship and thanks Guillermo Moyna, Michael Pak, Kadir Diri, and Ken Jordan for helpful discussions and Kenneth Ruud for assistance with the DALTON calculations. Q. W. thanks Mark Tuckerman for helpful discussions and assistance using the PINY_MD simulation package.

Supporting Information Available: Tables of vibrational frequencies and structural parameters and a figure of *n*-order terms for the HF dimer calculated at the MP2/aug-cc-pVTZ level of theory. This material is available free of charge via the Internet at http:// pubs.acs.org.

References and Notes

(1) Pavese, M.; Chawla, S.; Lu, D. S.; Lobaugh, J.; Voth, G. A. *J. Chem. Phys.* **1997**, *107*, 7428.
(2) Tuckerman, M. E.; Marx, D.; Klein, M. L.; Parrinello, M. *Science* **1997**, *275*, 817.
(3) Diri, K.; Myshakin, E. M.; Jordan, K. D. *J. Phys. Chem. A* **2005**, *109*, 4005.
(4) Schenter, G. K.; Garrett, B. C.; Voth, G. A. *J. Chem. Phys.* **2000**, *113*, 5171.
(5) Minikis, R. M.; Jensen, J. H. *Int. J. Quantum Chem.* **2000**, *76*, 341.
(6) Raugei, S.; Klein, M. L. *J. Am. Chem. Soc.* **2003**, *125*, 8992.
(7) Chen, B.; Ivanov, I.; Klein, M. L.; Parrinello, M. *Phys. Rev. Lett.* **2003**, *91*, 215503.
(8) Gregory, J. K.; Clary, D. C. *J. Phys. Chem.* **1996**, *100*, 18014.
(9) Clary, D. C.; Benoit, D. M.; van Mourik, T. *Acc. Chem. Res.* **2000**, *33*, 441.
(10) Astrand, P.-O.; Karlstrom, G.; Engdahl, A.; Nelander, B. *J. Chem. Phys.* **1995**, *102*, 3534.
(11) Swalina, C.; Hammes-Schiffer, S. *J. Phys. Chem. A* **2005**, *109*, 10410.
(12) Guedes, R. C.; Do Couto, P. C.; Costa Cobral, B. J. *J. Chem. Phys.* **2003**, *118*, 1272.
(13) McCoy, A. B.; Huang, X. C.; Carter, S.; Landeweer, M. Y.; Bowman, J. M. *J. Chem. Phys.* **2005**, *122*, 061101.
(14) Diken, E. G.; Headrick, J. M.; Roscioli, J. R.; Bopp, J. C.; Johnson, M. A.; McCoy, A. B. *J. Phys. Chem. A* **2005**, *109*, 1487.
(15) Howard, B. J.; Dyke, T. R.; Klemperer, W. J. *J. Chem. Phys.* **1984**, *81*, 5417.
(16) Weis, P.; Kemper, P. R.; Bowers, M. T.; Xantheas, S. S. *J. Am. Chem. Soc.* **1999**, *121*, 3531.
(17) Peterson, K. A.; Dunning, T. H., Jr. *J. Chem. Phys.* **1995**, *102*, 2032.
(18) Car, R.; Parrinello, M. *Phys. Rev. Lett.* **1985**, *55*, 2471.
(19) Marx, D.; Tuckerman, M. E.; Martyna, G. J. *Comput. Phys. Commun.* **1999**, *118*, 166.
(20) Tuckerman, M. E.; Marx, D.; Klein, M. L.; Parrinello, M. *J. Chem. Phys.* **1996**, *104*, 5579.
(21) Barone, V. *J. Chem. Phys.* **2004**, *120*, 3059.
(22) Barone, V. *J. Chem. Phys.* **2005**, *122*, 014108.
(23) Tuckerman, M. E.; Martyna, G. J. The PINY_MD Simulation Package.
(24) Tuckerman, M. E.; Yarne, D. A.; Samuelson, S. O.; Hughes, A. L.; Martyna, G. J. *Comput. Phys. Commun.* **2000**, *128*, 333.
(25) Streng, A. G. *J. Chem. Eng. Data* **1971**, *16*, 357.
(26) Troullier, N.; Martins, J. L. *Phys. Rev. B* **1991**, *43*, 1993.
(27) Frisch, M. J.; Trucks, G. W.; Schlegel, H. B.; Scuseria, G. E.; Robb, M. A.; Cheeseman, J. R.; Montgomery, J. A., Jr.; Vreven, T.; Kudin, K. N.; Burant, J. C.; Millam, J. M.; Iyengar, S. S.; Tomasi, J.; Barone, V.; Mennucci, B.; Cossi, M.; Scalmani, G.; Rega, N.; Petersson, G. A.; Nakatsuji, H.; Hada, M.; Ehara, M.; Toyota, K.; Fukuda, R.; Hasegawa, J.; Ishida, M.; Nakajima, T.; Honda, Y.; Kitao, O.; Nakai, H.; Klene, M.; Li, X.; Knox, J. E.; Hratchian, H. P.; Cross, J. B.; Adamo, C.; Jaramillo, J.; Gomperts, R.; Stratmann, R. E.; Yazyev, O.; Austin, A. J.; Cammi, R.; Pomelli, C.; Ochterski, J. W.; Ayala, P. Y.; Morokuma, K.; Voth, G. A.; Salvador, P.; Dannenberg, J. J.; Zakrzewski, V. G.; Dapprich, S.; Daniels, A. D.; Strain, M. C.; Farkas, O.; Malick, D. K.; Rabuck, A. D.; Raghavachari, K.; Foresman, J. B.; Ortiz, J. V.; Cui, Q.; Baboul, A. G.; Clifford, S.; Cioslowski, J.; Stefanov, B. B.; Liu, G.; Liashenko, A.; Piskorz, P.; Komaromi, I.; Martin, R. L.; Fox, D. J.; Keith, T.; Al-Laham, M. A.; Peng, C. Y.; Nanayakkara, A.; Challacombe, M.; Gill, P. M. W.; Johnson, B.; Chen, W.; Wong, M. W.; Gonzalez, C.; Pople, J. A. *Gaussian03*, revision C.03 ed.; Gaussian, Inc.: Pittsburgh, PA, 2003.
(28) Becke, A. D. *Phys. Rev. A* **1988**, *38*, 3098.
(29) Lee, C.; Yang, W.; Parr, P. G. *Phys. Rev. B* **1988**, *37*, 785.
(30) Becke, A. D. *J. Chem. Phys.* **1993**, *98*, 5648.
(31) Stephens, P. J.; Devlin, F. J.; Chablowski, C. F.; Frisch, M. J. *J. Phys. Chem.* **1994**, *98*, 11623.
(32) Woon, D. E.; Dunning, T. H., Jr. *J. Chem. Phys.* **1993**, *98*, 1358.
(33) Astrand, P.-O.; Ruud, K.; Taylor, P. R. *J. Chem. Phys.* **2000**, *112*, 2655.
(34) Ruud, K.; Astrand, P.-O.; Taylor, P. R. *J. Chem. Phys.* **2000**, *112*, 2668.
(35) Ruud, K.; Astrand, P.-O.; Taylor, P. R. *J. Am. Chem. Soc.* **2001**, *123*, 4826.
(36) Helgaker, T.; Jensen, H. J. A.; Jorgensen, P.; Olsen, J.; Ruud, K.; Agren, H.; Andersen, T.; Bak, K. L.; Bakken, V.; Christiansen, O.; Dahle, P.; Dalskov, E. K.; Enevoldsen, T.; Fernandez, B.; Heiberg, H.; Hettema, H.; Jonsson, D.; Kirpekar, S.; Kobayashi, R.; Koch, H.; Mikkelsen, K. V.; Norman, P.; Packer, M. J.; Saue, T.; Taylor, P. R.; Vahtras, O. *Dalton, An ab Initio Electronic Structure Program*, 2.0 ed. (see http:// www.kjemi.uio.no/software/dalton/dalton.html, last accessed March 2005).
(37) Janzen, J.; Bartell, L. S. *J. Chem. Phys.* **1969**, *50*, 3611.
(38) Kreitmeir, M.; Heusel, G.; Bertagnolli, H.; Todheide, K.; Mundy, C. J.; Cuello, G. J. *J. Chem. Phys.* **2005**, *122*, 154511.
(39) Loewenstein, A.; Shporer, M.; Lauterbur, P. C.; Ramirez, J. E. *Chem. Commun.* **1968**, 214.
(40) Ubbelohde, A. R.; Gallagher, K. J. *Acta Crystallogr.* **1955**, *8*, 71.
(41) Bowman, J. M. *J. Chem. Phys.* **1978**, *68*, 608.
(42) Bowman, J. M. *Acc. Chem. Res.* **1986**, *19*, 202.
(43) Chaban, G. M.; Jung, J. O.; Gerber, R. B. *J. Chem. Phys.* **1999**, *111*, 1823.
(44) Chaban, G. M.; Gerber, R. B. *Spectrochim. Acta Part A: Mol. Biomol. Spectrosc.* **2002**, *58*, 887.
(45) Yagi, K.; Taketsuga, T.; Hirao, T.; Gordon, M. S. *J. Chem. Phys.* **2000**, *113*, 1005.
(46) Schmidt, M. W.; Baldridge, K. K.; Boatz, J. A.; Elbert, S. T.; Gordon, M. S.; Jensen, J. H.; Koseki, S.; Matsunaga, N.; Nguyen, K. A.; Su, S.; Windus, T. L.; Dupuis, M.; Montgomery, J. A. *J. Comput. Chem.* **1993**, *14*, 1347.
(47) Roscioli, J. R.; Diken, E. G.; Johnson, M. A.; Horvath, S.; McCoy, A. B. *J. Phys. Chem. A* **2006**, *110*, 4943.
(48) Allen, M. P.; Tildesley, D. J. *Computer Simulation of Liquids*; Clarendon Press: Oxford, 1989.
(49) Finchamm, D.; Quirke, N.; Tildesley, D. J. *J. Chem. Phys.* **1986**, *84*, 4535.